AIAA SciTech Forum
6-10 January 2025, Orlando, FL
AIAA SCITECH 2025 Forum

10.2514/6.2025-2058

Characterization the Anti-Icing and Performance and Rain-Erosion Resistance of a Superhydrophobic Coating for UAV Icing Mitigation

Carlos Valentin[1], Harsha Sista[2], Anvesh Dhulipalla[2], Amrit Kumar[3], Abdallah Samad[3] and Hui Hu[4]
Department of Aerospace Engineering, Iowa State University, Ames, Iowa, 50011

An experimental study is conducted on a superhydrophobic coating (WX 2100) to characterize the glaze ice accretion characteristics and understand the rain erosion effects. This study is performed using the unique Icing Research Tunnel (IRT), and the rain erosion testing rig available at Iowa State University. Hybrid anti-icing tests were performed by using a heating element to cover 10% of the chord length, and the entire model was coated with the WX 2100 coating to facilitate water runback. Measurement results indicate that an applied power density of 4.5 kW/m^2 to the thermal film was enough to make the entire surface of a UAV airfoil/wing model ice-free for the superhydrophobic coating, in contrast to at least 25kW/m^2 required for the enamel hydrophilic surface. To characterize the coating durability, the static, advancing, and receding contact angles, as well as the ice adhesion strength, are measured before and after rain erosion tests, given that both variables are a function of the duration of the rain erosion testing. A decrease in the contact angle and surface roughness, along with an increase in ice adhesion, was observed throughout 60 minutes of accelerated rain erosion at 80 m/s with LWC = 16.0 g/m^3.

I. Introduction

Unmanned Air Vehicles (UAV) have been an exceptional development in the aviation industry due to their remote or autonomous controllability and have proven their importance in the engineering community for civilian and military applications. UAVs can be used for surveillance operations, film shooting, agriculture, cargo transport, healthcare, search and rescue, and scientific research. UAVs can operate for extended periods and venture into hazardous and remote locations without the risk of putting onboard pilots in danger [1]. This promotes casualty reduction and cost-effectiveness to military applications which is attractive to engineering and, as a result, sees the widespread adoption of UAVs throughout the industry. However, small and mid-sized UAVs operating in cold climates are much more susceptible to icing situations compared to larger, manned air vehicles due to a lower cruising altitude and higher liquid water content (LWC). They also typically operate at a much slower speed, which results in longer exposure to icing conditions. For now, UAVs are considered inoperable in cold climates due to the potential damage inflight icing can cause [2]. Hydro-/ice-phobic coatings provide a possible solution to safe UAV operations in cold climates where the current best approach to mitigate icing conditions for UAVs is mission cancellations and grounding.

For icing mitigation, active anti/de-icing methods include chemical fluid spraying, thermal heating, and mechanical removal, all of which suffer from high energy consumption, low efficiency, and a high need for resources. Therefore, they cannot solely be considered for small-scale systems due to the limited payload [3]. Factors to be noted when searching for an effective anti-icing method are weight, complexity, and effectiveness. In contrast, passive methods have no external energy input since they mainly consist of anti-icing materials (AIM) or coatings on the UAV wing surface to prevent ice accumulation. Some of the common coatings are hydrophobic, with contact angles larger than 90°, and super-hydrophobic surfaces, with contact angles larger than 150° [4]. These coatings usually have low ice

[1] PhD Student, Department of Aerospace Engineering,
[2] PhD Candidate, Department of Aerospace Engineering,
[3] Postdoctoral Research Associate, Department of Aerospace Engineering.
[4] Anson Marston Distinguished Professor, Department of Aerospace Engineering, AIAA Associate Fellow. Email: huhui@iastate.edu

adhesion strength and good mechanical durability to reject ice accretion. These coatings aim to repel incoming water droplets, suppress ice nucleation, and lower ice adhesion strength [6]. In Fig. 1, we can observe the physical difference of droplets on the mentioned surfaces compared to hydrophilic and super-hydrophilic surfaces.

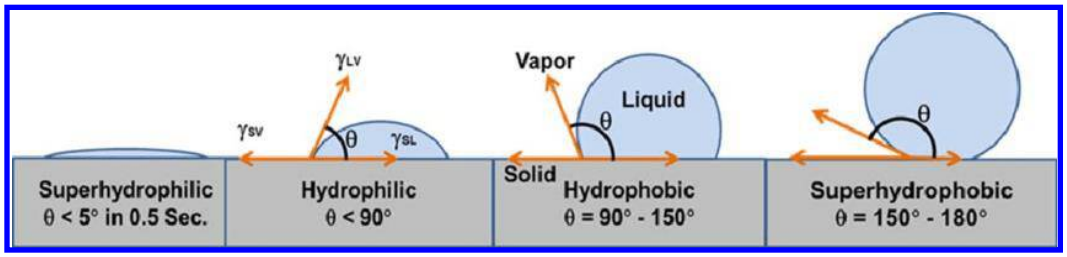

Figure 1: Schematic view of super-hydrophilic, hydrophilic, hydrophobic, and super-hydrophobic surfaces [5].

Passive anti-icing has gained more attention over recent years as a viable strategy for icing mitigation. The development of superhydrophobic coatings is inspired by the self-cleaning capability of duck feathers and lotus leaves, which results in droplets beading up and dripping off rapidly from an inclined surface, as seen in Fig. 2. This natural phenomenon has led to studies to create coatings with the ability to repel supercooled droplets and snow/ice [7-9]. Some examples of these coatings include Super-hydrophobic surfaces (SHS) [5,11] and Slippery liquid-infused porous surfaces (SLIPS) [10,11], which have several extensive studies that demonstrate the effectiveness of this developed anti-icing technology. The coating used in this study is WX 2100, which has superhydrophobic properties, including the elimination of water film formation, reduces ice and snow adhesion, and causes water to roll off, leaving the surface dry. The main application of this coating is to prevent signal loss due to rain, ice, and snow on satellite dishes and antenna arrays. It is specifically used on marine and ground-based microwave antennas, and other telecommunication gear. However, the properties of this coating can easily translate to aerospace applications due to the super**h**ydrophobic qualities they possess. WX 2100 provides a contact angle performance of over 140°, which is ideal for the study [21]. The WX 2100 coating was sprayed from the can at a 6-inch distance for 4-5 layers on each test sample.

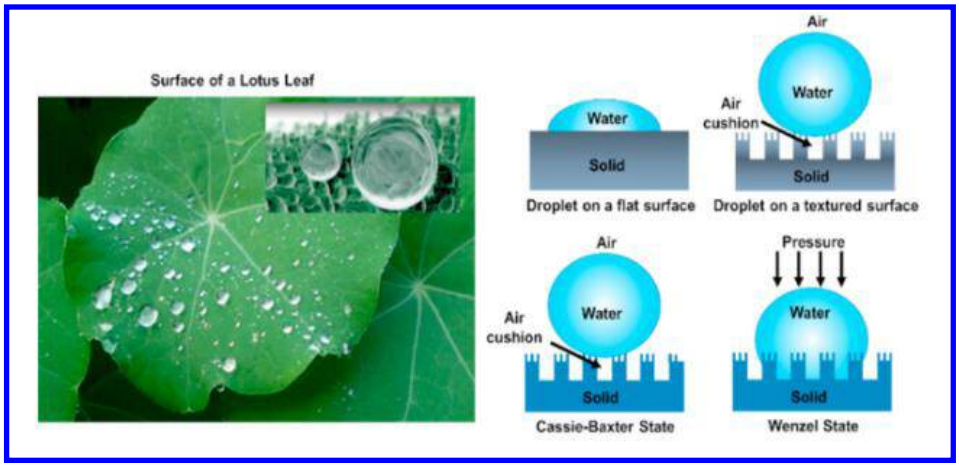

Figure 2: Similarity of Super-hydrophobic coatings to the lotus leaf and the variation of states droplets could undergo [10].

A valued method for testing the durability of a coating is rain erosion testing. The fundamental idea of rain erosion involves the damage caused to a solid surface as droplets impinge on the surface continuously over time [12]. While water is theoretically incompressible, water droplets can be compressible at the initial stage of the impingement process, generating a shock wave at the solid-liquid interface [13]. This is called the water hammer effect, which generates water hammer pressure that is a function of the droplet impingement velocity and the liquid and solid physical properties, which can be observed in Eq. (1) [14-15]. This equation defines the water hammer pressure P_H as a function of U_∞ , which is the impacting speed of the droplet, ρ_L, and ρ_S are the density of the liquid and solid substrate,

and c_L and c_S are the speed of sound in the liquid and solid, respectively. As seen in Fig. 3, while the generated shock wave at the initial impingement zone (highlighted in blue) propagates, longitudinal Rayleigh and transverse bulk waves are also generated. These propagate along the surface and into the substrate.

$$P_H = \rho_L c_L U_\infty \left(\frac{1}{1 + \frac{\rho_L c_L}{\rho_s c_s}} \right) \tag{1}$$

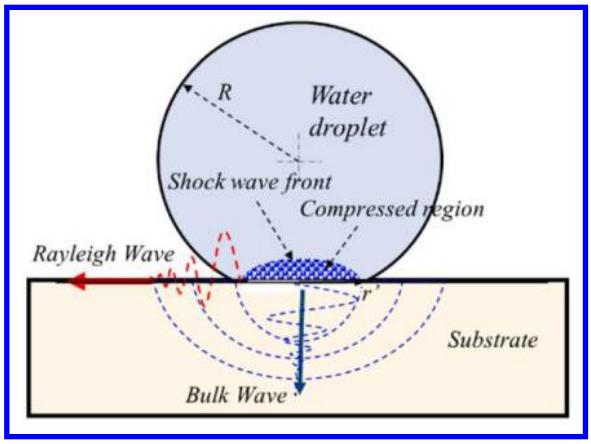

Figure 3: Rain erosion mechanism after impacting a droplet onto the surface [6].

The Rayleigh and Bulk waves are unimportant in the initial stage of the droplet impingement since the moving speed of the contact edge moves faster than the wave propagation, making the "water hammer effect" much more powerful. However, the moving speed of the contact edge slows down as the droplet spreads across the surface which is mainly a result of the liquid viscosity and friction force of the substrate. As a result, the Rayleigh and Bulk Waves become more dominant and promote material degradation [12]. To test the durability of coated test plates, intermittent surface wettability measurements would have to take place during the rain erosion testing to track the effectiveness of the coating as the degrading progresses.

Although the effectiveness of these coatings is apparent, there are some limitations to solely using this anti-icing method. All coatings degrade over time due to environmental exposure, such as constant droplet impingement from rain and snow and ambient temperature cycling. This would lead to performance degradation, where thawing the ice from the surface and frequent re-application would be necessary, increasing maintenance costs. They are effective at delaying ice formation ascribable to the surface properties; however, removing the ice manually can cause mechanical wear, which would reduce the water-repellency effect of the coating. As ice accumulation begins, the advantage of these coatings is lost, and icing on the leading edge would be evident. For this reason, hybrid anti-icing methods (thermal heating and coating application combined) are a possible solution to mitigate these icing issues.

It is known that the high-power consumption from the use of thermal heating as an anti-icing method is significant, and potential overheating of the composite blades is also a risk. To address these challenges, the hybrid method could be introduced as the high convective heat transfer provided by the thermal heating (mainly on the leading edge since this is the primary target of the droplets), together with the water-repelling coating, would complement each other's advantages. The heat transfer on the leading edge would prevent ice accumulation by melting any ice that impacts the blade. The risk of water repellency reduction due to wear or degradation would be mitigated. Meanwhile, the coating would sustain surface properties for a longer duration of time and would continue to repel water across the chord of the blade. Thermal heating alone may cause slower droplet movement towards the trailing edge (runback), leading to refreezing. To address this issue, the proposed coatings would accelerate the runback water (preventing the droplets from adhering to the surface), ensuring shedding before refreezing [7], reducing the amount of area needed for heating, and improving the overall energy consumption. This phenomenon is more prevalent in hydrophilic surfaces where it is preferable to heat the entire chord of the blade due to the lack of water-repellency properties. Thermal heating can also potentially reduce the wear-off time since continuous heating on the leading edge prevents ice build-up.

Therefore, there is less chance of mechanical abrasion or overall damage to the coating from ice accretion and shedding. The combination of these methods would create a hybrid synergy between both anti-icing techniques, increasing the efficiency of the icing mitigation. The present study focuses on testing the effectiveness of the hybrid method in addition to characterizing the degradation and durability of the coating.

II.Experimental Setup and Test Model

A. Hybrid Testing of a Combined Active & Passive Ice Protection System for Fixed Wings

An experimental study was performed in the Icing Research Tunnel at Iowa State University (i.e., ISU-IRT in Fig. 8) to test anti/de-icing with dual methods (passive anti-icing with thermal heating). The ISU-IRT is a multi-functional icing tunnel with a test section of 2.0m in length x 0.4m in width x 0.4m in height, with four side walls being optically transparent. The icing tunnel can run at a maximum wind speed of 100 m/s and a minimum airflow temperature of -25°C. Nine pneumatic atomizer/spray nozzles are installed before the contraction section of the ISU-IRT to inject supercooled water droplets into the airflow and onto the leading edge at the test section. The Median Volume Diameter (MVD) of these droplets is approximately 20 µm. The liquid water content can be manipulated within a range of 0.1 and 10 g/m^3 [16,17,18,19]. An S1223 airfoil profile with a chord length of C = 0.19 m and a spanwise length of L = 0.40 m is used in the present study for testing anti/de-icing effects. The material used to manufacture this model was ABS, mainly used for drones, UAVs, and polymer-based modern aircraft. Also displayed in Fig. 4, an electric film heater (i.e., DuPont^{TM} Kapton$^{®}$ film heater with 50µm thickness) was wrapped around the S1223 airfoil's leading edge at 10% chord. This film is covered with Kapton tape, coated with the hydrophilic enamel coating, and finally coated with WX-2100. This airfoil model preparation was inspired by the methodology used by Digavalli et al. [20]. The test conditions of all icing experiments included glace ice at T = -5°C, LWC = 2 g/m^3, V = 20 m/s, and a variation of power density for the heating film set from 0 to 20 kW/m^2. Type K thermocouples were added to the S1223 airfoil model to analyze the temperature distribution across the chord during heating and icing stages at the leading edge (LE), 10% chord, 25% chord, 50% chord, and the trailing edge (TE).

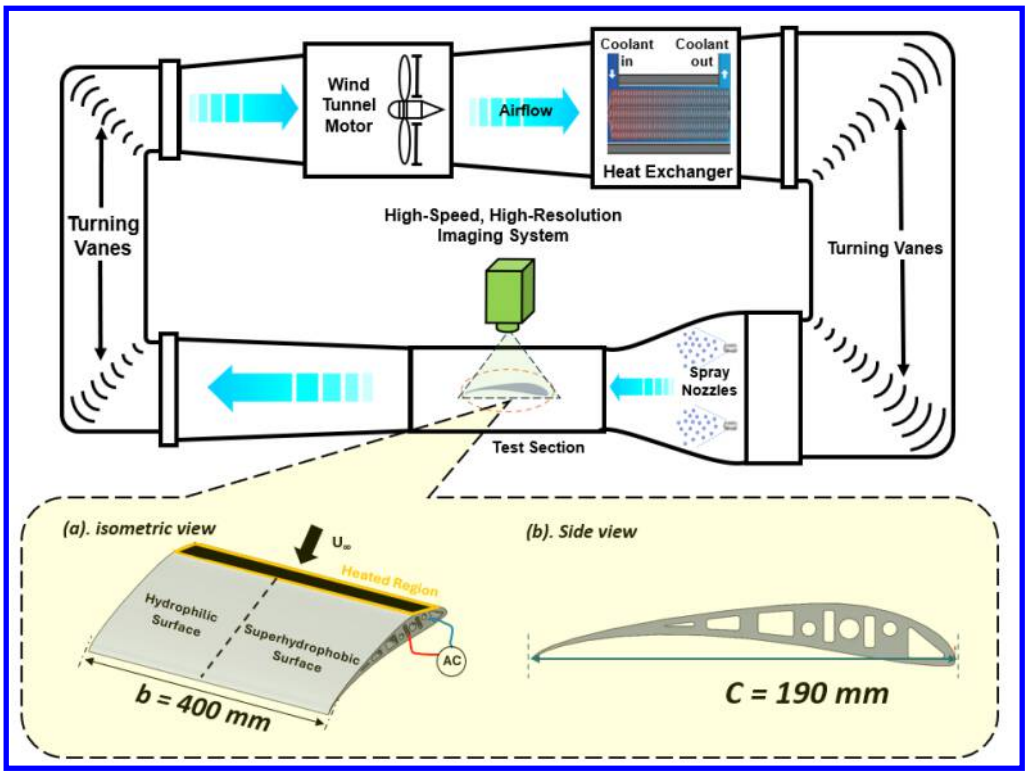

Figure 4: Schematic of the IRT-ISU used for airfoil testing and test model.

B. Particle Image Velocimetry (PIV) Measurement Technique

Another technique used in this study was high-resolution digital particle image velocimetry (PIV). This technique helps ensure the uniformity of the impacting fluid onto the test sample during the rain erosion testing and quantifies the droplet speed for validation. The speed used for these degradation experiments was $U_\infty = 80$ m/s. The water droplets themselves were used as the seeding particles, and an Nd-YAG 532 nm laser was used as the illumination source. A high-speed camera (Photron Fastcam Mini WX100) would record these illuminated droplets as they impact the surface. The schematic of the experimental set-up for PIV can be seen in Fig. 5. Image processing was done in DaVis (an image acquisition software), obtaining the velocity profiles from nozzle exit to test sample and along the vertical plane of the nozzle exit. Tecplot 360 was used to acquire the velocity vectors across the entire fluid and the physical velocity profile as it impacts the test sample.

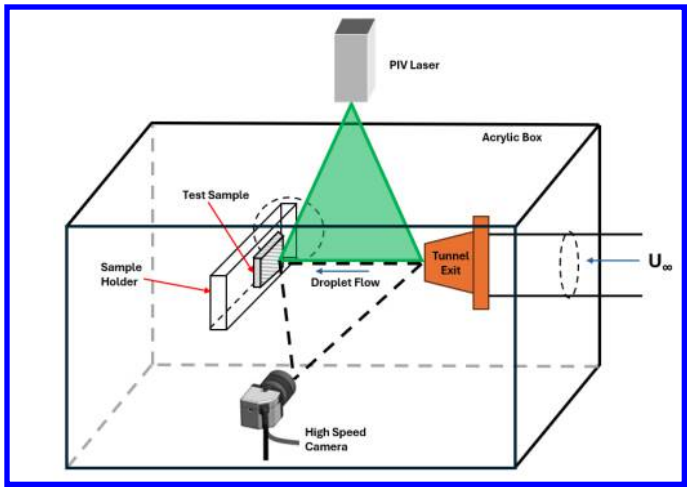

Figure 5: Schematic of the PIV testing set-up in the Rain Erosion Tunnel test section.

C. The Rain Erosion Testing Rig

To test the durability of the coatings, surface wettability, surface roughness, and ice adhesion strength of the considered substrates used on UAV wing surfaces are examined. These coatings undergo continuous water droplet impingement (simulating rain erosion effects) at high speeds (80 m/s) for accelerated testing. The rain erosion test rig at Iowa State University (Fig. 6) is specially designed for this study and can generate the required air jet flow and micro-sized water droplets with a variation of liquid water content (LWC). A high-thrust electric ducted fan (EDF, JP Hobby) drives the airflow towards the outlet (20.3mm at the nozzle outlet), with adjustable speed, by controlling the fan's power, for which a calibration curve was done. A water spray nozzle (BIMV-11002), with a droplet range of 20-100 microns, was integrated into the midsection of the rig for micro-sized deionized water droplet injection into the airflow. The water flow rate can also be adjusted to vary the LWC levels to simulate different test conditions. Additionally, the air pressure of the nozzle was limited to maintain the droplet size at 20 microns.

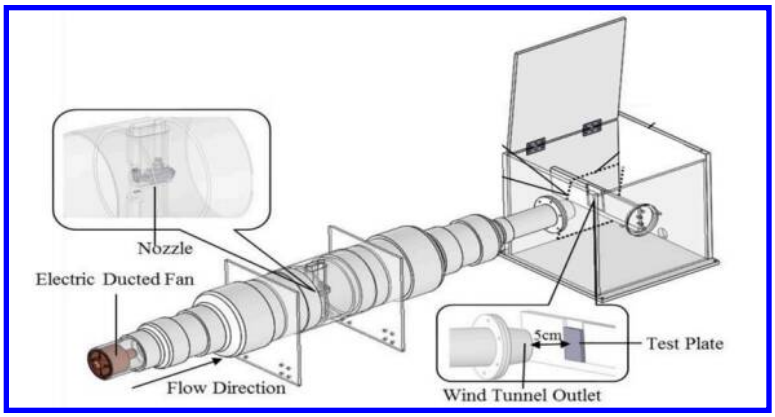

Figure 6: Schematic of the rain erosion testing rig at Iowa State University [5].

D. Contact Angles and Ice Adhesion Strength Measurement Techniques

Surface Wettability on a coated test plate can be measured through the length of the rain erosion testing by measuring the static contact angles (CA, θ_{static}), advancing CA (θ_{adv}), and the receding CA (θ_{rec}) of the water droplets on the test plates. The experimental setup to measure the contact angles can be seen in Fig. 8, which was inspired by the needle-in-the-sessile-drop method described in Korkoneen et al. (2013) [22]. The θ_{static} requires placing sessile water droplets (~50µL) on the test plate and measuring the contact angle, as seen in Fig. 7. The θ_{adv} and θ_{rec} consist of expanding and contracting the water droplets with a rate of 10µL/s. This flow rate is controlled by a programmable syringe pump (Genie Touch). This procedure is recorded with a digital camera (PCO2000, with a 2000 x 2000-pixel resolution) and a 12x zoom lens system (LaVision) to observe static and dynamic CA's. These images would be processed using a custom MATLAB code to measure the CA's. The coatings were also measured for surface roughness utilizing a Mitutoyo SJ-210 series surface roughness tester that provided Ra and Rq values in micrometer units. Comparisons to an uncoated test plate sample would also be made to notice the differences in CA while running the rain erosion tests.

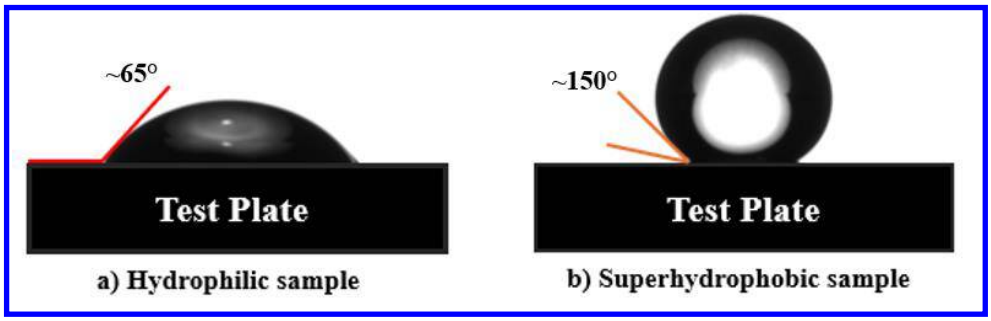

Figure 7: Demonstration of how the droplet would be measured on the test plates.

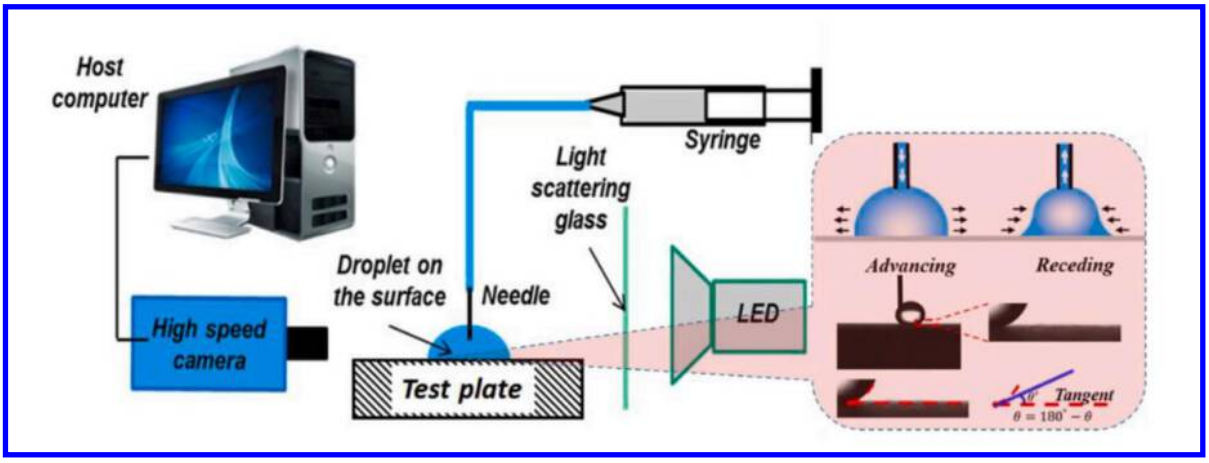

Figure 8: Experimental set-up to measure CA of droplets on the test plates [5].

Another measurement technique is evaluating variations in ice adhesion strength, τ_{ice}, on the test plates. This test is also done through the length of the rain erosion tests; Therefore, τ_{ice} measurements would be done apace with the CA measurements as the rain erosion testing progresses. The test plate containing the substrate is mounted in a temperature-controlled acrylic test chamber, with the surface maintained at -10°C using a Peltier Cold Plate. The test chamber is also kept at a cold temperature since it will be connected to a Styrofoam container filled with dry ice. To test τ_{ice}, four adhesion cylinders (D = 10mm) will be filled with deionized water onto the test plate at -10°C, letting the water freeze. The force transducer is set up parallel to the test plate to shear off the cylinders that froze upon the test plate, which will give us the force needed to calculate ice adhesion strength. A diagram of this set-up can be seen in Fig. 9. This experimental set-up was inspired by Beemer (2016) and Meuler (2010) [23][24]. The material of the substrate is ABS (Acrylonitrile Butadiene Styrene) coated with hydrophilic enamel paint and then sanded to 2000 grit. The contact angle measurements and ice adhesion strength of the enamel paint can be seen in Table 2, together with

the results of the superhydrophobic coatings. The superhydrophobic coatings will be painted onto the enamel, measured for contact angles and ice adhesion strength, and finally undergo rain erosion to analyze the degradation.

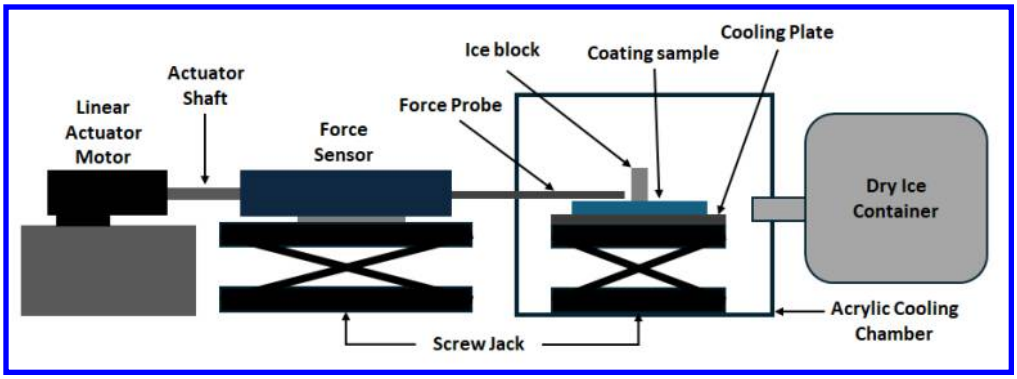

Figure 9: Experimental setup to measure ice adhesion strength on the test plates

III. Measurement Results and Discussions

A. Hybrid Anti-Icing Testing for Enamel &WX 2100 with Temperature Distributions

The anti-icing performance of the Enamel-coated ABS airfoil model combined with LE heating at 10% chord was evaluated under a variety of power densities, including 0 kW/m^2 (non-heated baseline), 4.5 kW/m^2, 14 kW/m^2, and 20 kW/m^2. All of these tests were done at glaze icing conditions (V_∞ = 20 m/s, T = -5°C, and LWC = 2 g/m^3). The text matrix of this experiment can be observed in Table 1. Under the baseline conditions, Fig 10(a), ice accretion developed rapidly, covering the surface with ice progressively up to about 30% chord over 180 seconds. This indicates that the enamel coating alone does not hinder ice formation, as expected. Under 4.5 kW/m^2 power density, Fig 10(b), ice accretion developed rapidly, covering the surface with ice progressively up to about ~70% chord over 180 seconds indicating that the power density is not high enough to melt the water off from the airfoil. At a power density of 14 kW/m^2, Fig 10(c), ice formation is further mitigated with a more uniform melting pattern compared to the previous case. However, ice accumulation can still be observed at the TE and some at the LE indicating a near-complete ice-free surface but not fully effective. This displays that the 14 kW/m^2 power density condition is insufficient to fully prevent ice. With a power density of 20 kW/m^2, Fig 10(d), the melting pattern has been more effective but not enough to make the surface ice-free. This indicates that the amount of power density to have an ice-free surface on an Enamel coating should be at least 25 kW/m^2 which would exceed the thermal capability of the airfoil. These results correlate with the results seen in the Gao et al. paper [7], where we can see that the enamel coating alone cannot prevent ice formation, and there is highly limited ice prevention when thermally heating the coating as well.

The icing behavior on the S1223 airfoil coated with WX 2100 was tested for hybrid anti-icing combined with LE thermal heating at 10% chord also at glaze icing conditions (V_∞ = 20 m/s, T = -5°C and LWC = 2 g/m^3). The power densities used for this case were 0 kW/m^2 (non-heated baseline), 2 kW/m^2, 4 kW/m^2 and 4.5 kW/m^2. Under the no heating condition, Fig. 11(a), the ice accumulated rapidly towards the 30% chord region on the coated surface which shows that the hydrophobic properties of WX 2100 alone are insufficient under severe icing conditions. At a low power density of 2 kW/m^2, seen in Fig 11(b), ice formation is visibly delayed but fails to reach ice free conditions given that the surface still covered a significant portion of the airfoil at about 25% chord by 180 seconds. At 4 kW/m^2, Fig. 11(c), a major improvement in ice prevention is displayed where there is barely any ice for about 120 seconds. This indicates the beginning of the threshold of the ice-free condition for this method. Increasing the power density to 4.5 kW/m^2, Fig 11(d), the surface is completely ice-free, meaning that the rest of the power densities going forward will evidently be ice-free (as can be seen in Fig 10 to the left with 14 kW/m^2). This confirms the combination of the WX 2100 with moderate thermal heating effectively prevents ice formation by leveraging the water-repellent properties of the coating to enhance the melting and runback properties of the thermal heating method. This also would reduce power consumption when using stand-alone thermal heating methods. The power saving percentage when transitioning from Enamel at 25 kW/m^2 to WX 2100 at 4.5 kW/m^2 would be 82%. A summary of the test matrix and results can be observed in Table 1.

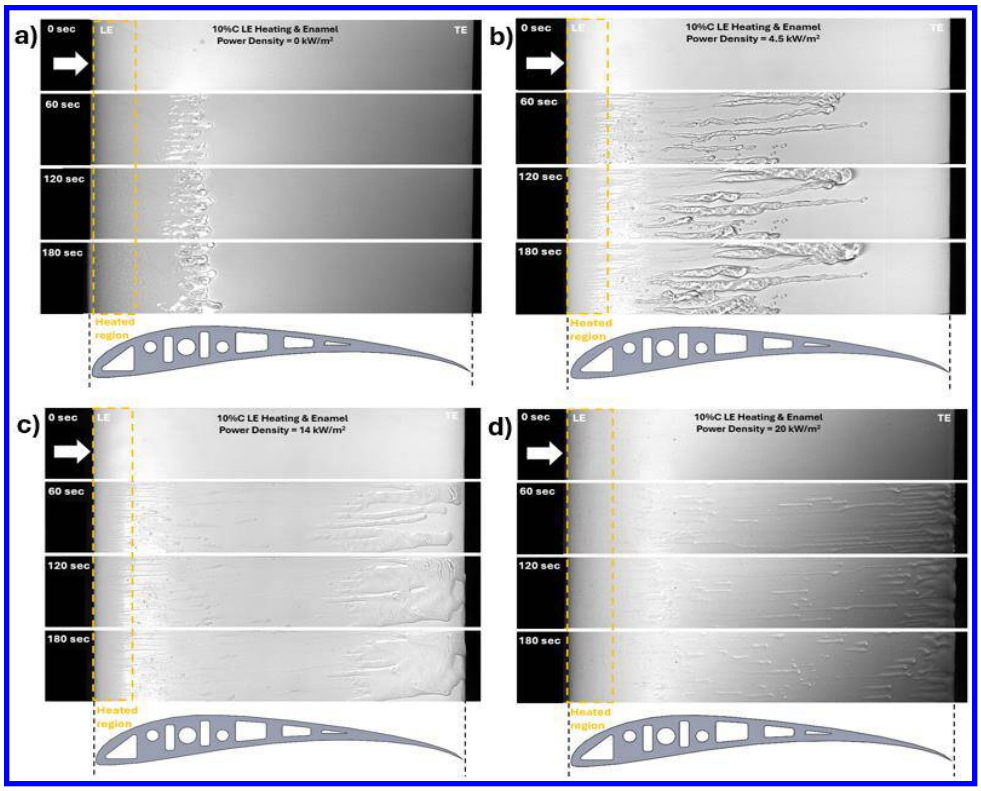

Figure 10: Hydrophilic coating results in Hybrid Anti-Icing testing.

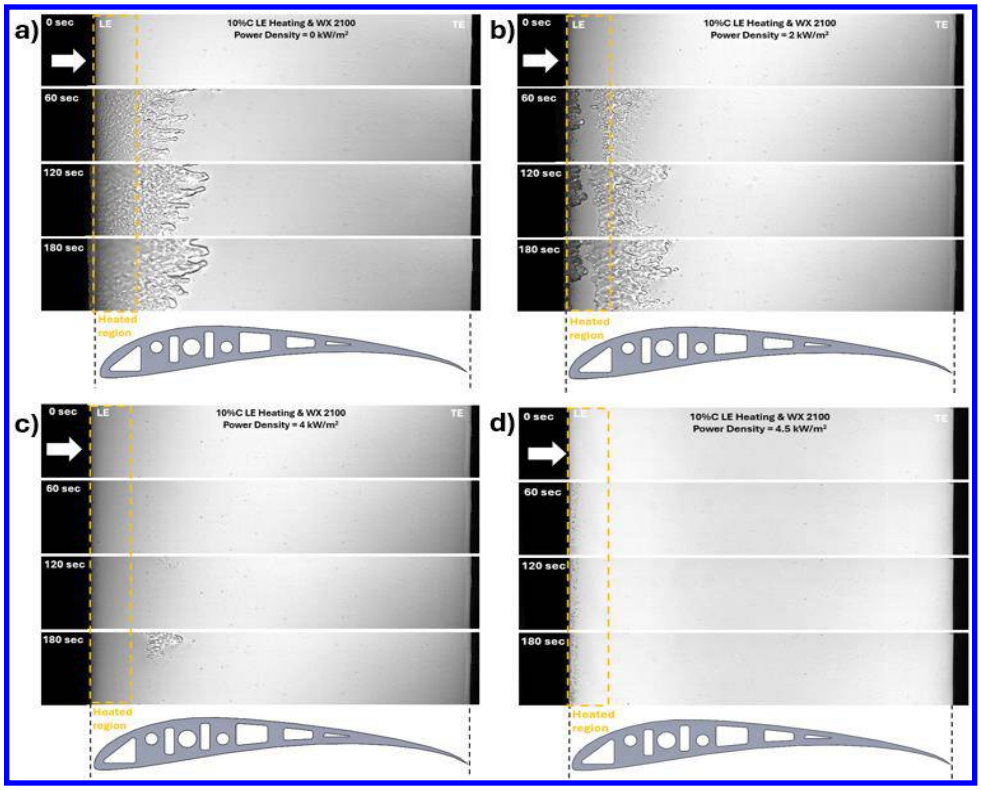

Figure 11: Hydrophobic coating results in Hybrid Anti-Icing testing.

Table 1: Test Matrix and Results from Hybrid Anti-Icing Test at Glaze Icing Conditions.

Case No.	Airflow Velocity (m/s)	LWC (g/m^3)	Temperature (°C)	Icing Time (min)	Power Density (kW/m^2)	WX 2100 Ice Free	Enamel Ice Free
1	20	2.0	-5	3	0	No	No
2	20	2.0	-5	3	2	Yes	No
3	20	2.0	-5	3	4	No	No
4	20	2.0	-5	3	4.5	Yes	No
5	20	2.0	-5	3	14	Yes	No
6	20	2.0	-5	3	20	Yes	No

The temperature distribution across the chord of the airfoil was analyzed for the uncoated (Fig. 12 on left) and coated (Fig. 12 on right) samples at a power density of 4.5 kW/m^2. The temperature difference (ΔT) is calculated by taking every data point and subtracting it from the trailing edge temperature, which corresponds to the free stream temperature. The heating element was run for 4 minutes to reach thermal equilibrium, followed by 3 minutes under icing conditions when the nozzles were turned on. The heating stage has a similar trend for both uncoated and coated, where the TE measurements remain at 0°C while the 50% chord measurements are approximately 0°C for heating and icing. The temperature noticeably begins to rise at 25% chord for the coated sample and fluctuates a bit for the uncoated sample. However, both temperatures for the 25% chord stabilize to zero by the end of the test. The LE and 10% chord temperature profiles on both samples have a similar trend, but the coated sample seems to gain a higher difference in temperature after the spray turns on and declines towards 5°C. This could indicate that the uncoated sample has a higher sensitivity to the water droplet temperature, given that the trend declines at 10% chord towards 0°C as the test continues. The coated sample fluctuates at the LE but maintains temperature after some time at approximately 25°C.

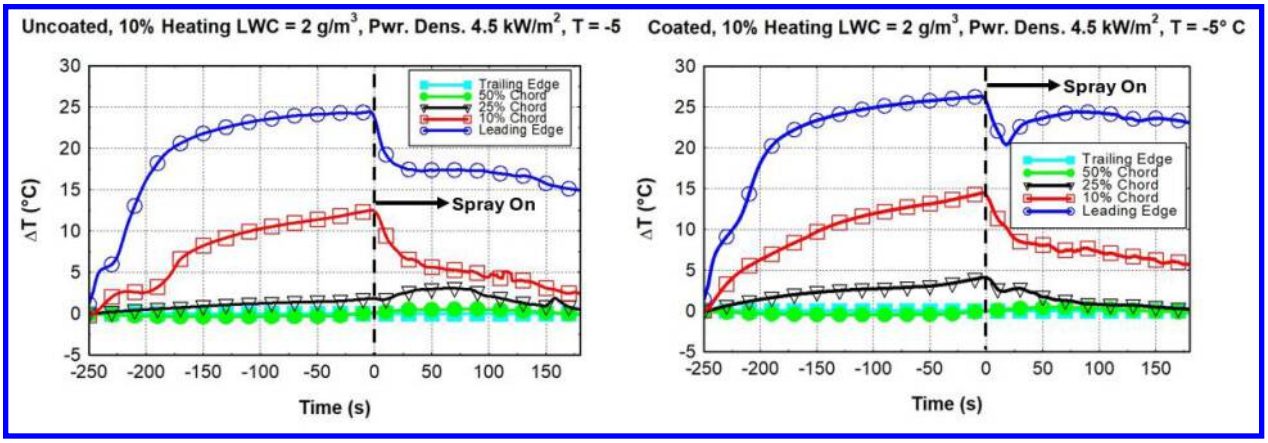

Figure 12: Type K Thermocouple measurement results for 4.5 kW/m^2 power density in Hybrid Anti-Icing testing.

With a higher power density of 14 kW/m^2, all temperatures rise significantly in comparison to the previous case. The TE remains at 0ºC in both heating and icing stages for uncoated and coated sides of the airfoil. The 50% chord rises for both stages slightly but is still similar to the TE temperature, maintaining stabilization close to 0ºC in heating and icing. At 25% chord, the uncoated side rises towards 10ºC at the end of the heating stage before decaying to <5C after the icing stage. The coated sample has a higher increase in temperature to about 15ºC at heating and stabilizes similarly to the uncoated sample. For the 10% chord measurements, there is a noticeable difference during heating between

uncoated and coated peaking at ~37ºC and ~40ºC, respectively. Both coatings stabilize to about the same temperature at 15C. The LE displays the highest difference between the surfaces, as the uncoated section rises to approximately 65ºC during heating while the coated sample increases towards 85ºC. The coated sample seems to stabilize to about 57ºC as the test ends, while the uncoated sample ends the spray stage with a temperature of 45ºC. This indicates that the coated surface retains heat more effectively than the uncoated surface due to its water-repellent properties.

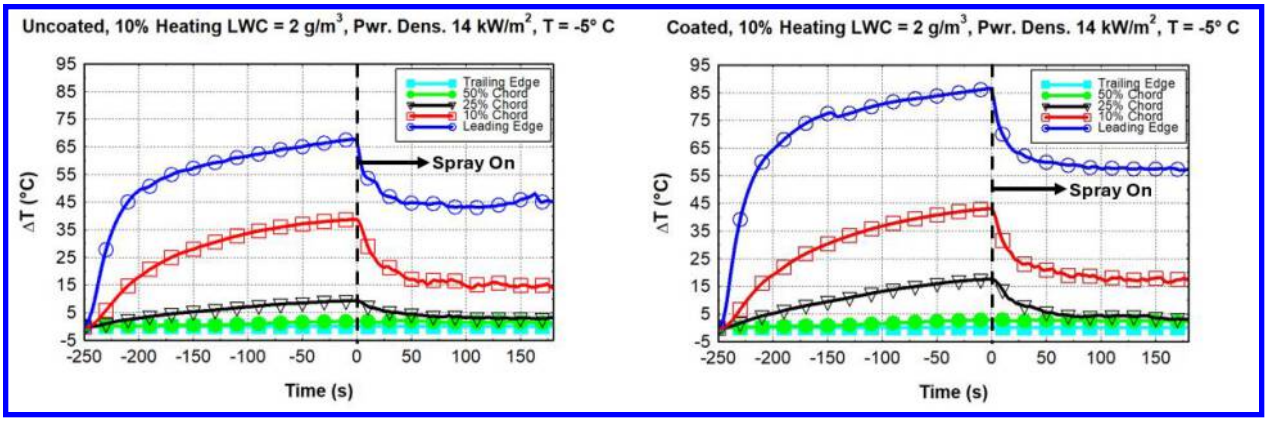

Figure 13: Type K Thermocouple measurement results for 14 kW/m^2 power density in Hybrid Anti-Icing testing.

B. PIV Measurements of the Spray Nozzle & Flow Characteristics

A typical PIV raw image is shown in Fig. 14(a), while the cross-correlated velocity profile is shown in Fig. 14(b). This initial test was conducted at an airflow velocity of V = 80 m/s. This was performed to ascertain the uniformity of the incoming water jet and to quantify the speed of the water droplet at the location of the test plate. The transverse velocity of the profiles of water droplets was also measured using the PIV data at the wind tunnel nozzle, and they can be seen in Fig. 14(c). The velocity across the nozzle is rather uniform and is close to 80 m/s, which is the same velocity as the freestream. Fig. 14(d) displays the flying velocity of the water droplets along the direction of the spray flow approaching the test plate. The droplets begin to completely decelerate as they approach the test plate and eventually reach stagnant.

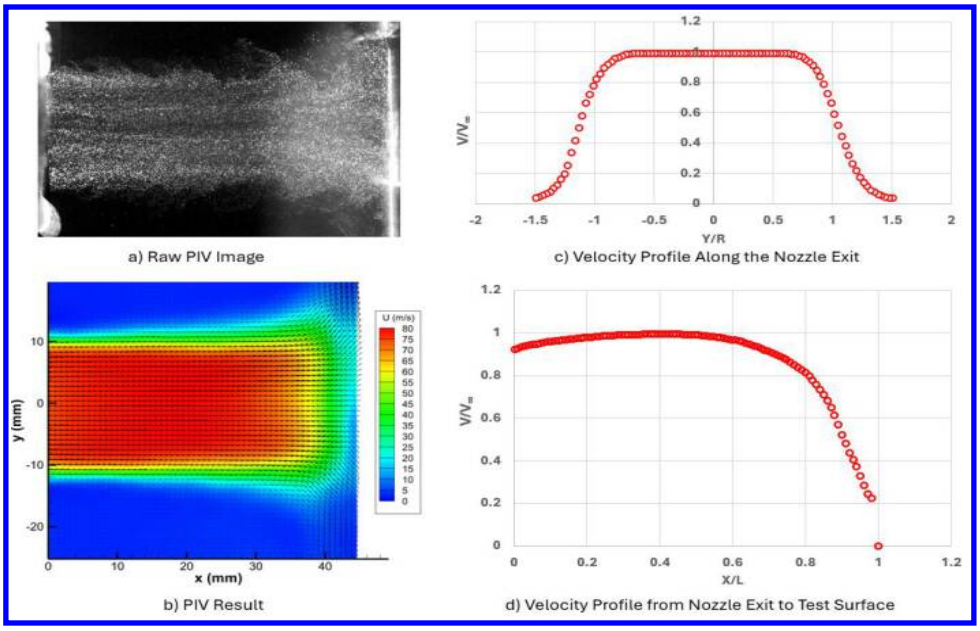

Figure 14: PIV measurements of the water jet impingement onto the test plate.

C. Surface Wettability Characterization: Contact Angle and Ice Adhesion

This method of surface wettability measurements has been tested previously by Zhang et al. and has proven effective in assessing the durability of AIM coatings [5,26]. They demonstrated the proof of concept by displaying static, $\theta_{adv,}$ and θ_{rec} measurements together with τ_{ice} of an SHS coating run at velocities from 45 to 100 m/s and at varied LWC levels. The degradation of the SHS coating at high velocities is evident from the increase in the τ_{ice} and the decrease in the CA's as the degradation progresses. The durability of the coatings can be observed to be higher at lower speeds, with minimal degradation or even non-existent, suggesting that the use of these coatings can be prolonged under these conditions.

This study was emulated by examining a CytoThane WX 2100 coating. For the present study, the experimental conditions were set to LWC =16 g/m^3 and V = 80 m/s. The θ_{static} *(SCA)*, θ_{adv} *(ACA)*, and θ_{rec} *(RCA)* measurements were observed as well as the τ_{ice}. Table 2 displays the parameters obtained for the substrates (coated and uncoated) before undergoing the rain erosion test [26].

Table 2: Substrate Parameters and Properties

Studied Surface	Wettability	Static CA (°)	Advancing CA (°)	Receding CA (°)	CAH value (°)	Ice Adhesion Strength (kPa)	Surface Roughness (microns)
Enamel Coated ABS	Hydrophilic	65	85	10	75	510	1.58
WX 2100	Hydrophobic	141.81	146.05	141.03	5.02	217	17.02

The degradation of both samples can be observed in the characterization; However, these experiments focused on a certain condition rather than the previous proof of concept that used several LWC levels and airflow velocities. Fig. 15 shows the static, advancing, and receding contact angle for the WX 2100 coating. The contact angle decreases with erosion time, which shows the degradation of the coating. The measurements for θ_{static} and θ_{adv} for WX 2100 begin at approximately 146° and continue to decrease to a range close to 138-140°. The measurement for θ_{rec} begins at a smaller value, approximately 141°, but continues to have a nearly identical decay towards 130°. Therefore, even with the rain erosion test completed, the coated sample continues to be hydrophobic after 60 minutes of testing since the CA values still exceed 90°. This proves that WX 2100 has reliable contact angle performance even with degradation, but the performance is not as effective as a fresh coating.

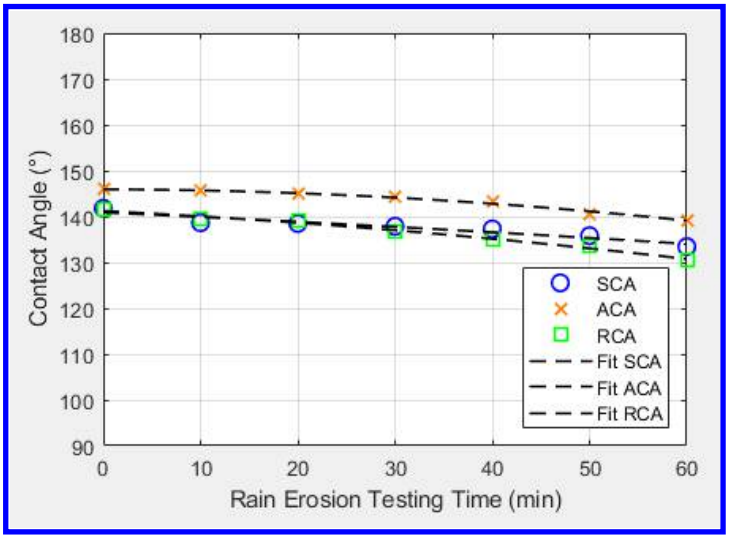

Figure 15: Measured θ_{sta}, $\theta_{adv,}$ and θ_{rec} vs. the time of the rain erosion testing for WX2100

From Fig. 16, we can see that the τ_{ice} is consistent with the coating degradation and shows a steady increase with time for all coatings. The ice adhesion for WX 2100 starts out at a low value (~200 kPa) and increases to ~450kPa by the end of the test. Therefore, from both the quantitative tests, we can conclude that the WX 2100 coating is effective immediately after application but will not be ideal for anti/de-icing applications once it starts degrading since 60 min of erosion testing is about a 60kPa difference from the Enamel baseline measurement.

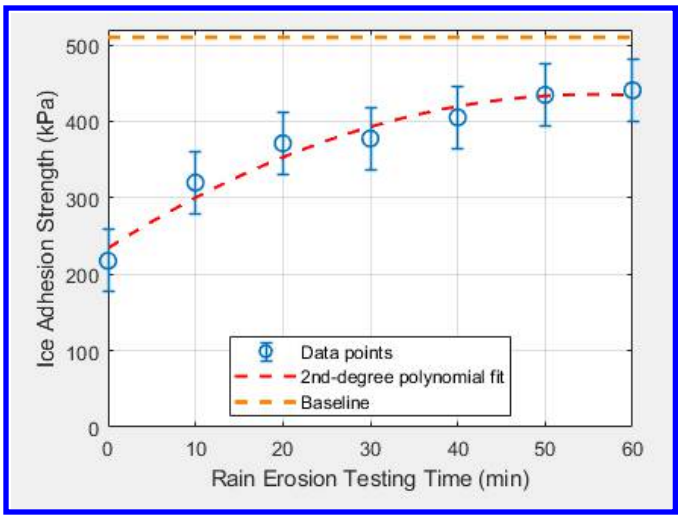

Figure 16: Measured ice adhesion strength (τ_{ice}) vs the time of the rain erosion testing for WX2100

D. Surface Roughness Measurements

The surface roughness plots, seen in Fig. 17, reveal the distinct erosion behaviors of WX 2100. Both Ra and Rq over the erosion time decreased consistently, indicating continuous surface degradation. Ra values started at 17 µm and lowered towards 9 μm. The Rq (root mean square roughness) initial value was 21 µm and lowered towards approximately 10 µm. Since Rq represents the average of the squares of the deviations of the surface profile, this determines how uniform the surface profile is. As can be seen, both Ra and Rq are relatively close in value (9 and 10 µm), suggesting that the surface is potentially uniform across the substrate. This can still be an indicator that the WX 2100 has slight resistance to extreme weather conditions due to the relatively high roughness of the surface since the surface is not entirely smooth.

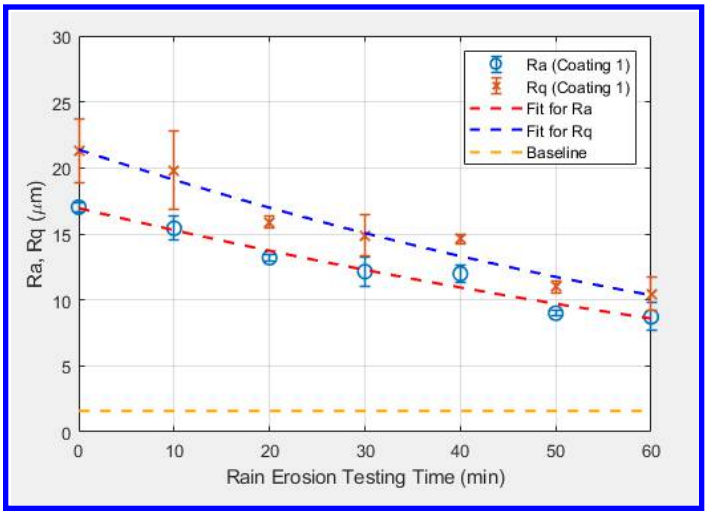

Figure 17: Measured surface roughness (Ra and Rq) vs the time of the rain erosion testing for WX2100

Conclusion

This study highlights the comparative performance of an enamel hydrophilic coating and the superhydrophobic WX 2100 coating for hybrid anti-icing applications in the Iowa State University Icing Research Tunnel. The tests were conducted for glaze icing conditions (V_∞ = 20 m/s, T = -5°C and LWC = 2.0 g/m^3). WX 2100 obtained ice-free conditions at significantly low power densities (4-5 kW/m^2) compared to the enamel-coated baseline case, which required at least 25 kW/m^2. These icing tests demonstrated the importance of using hybrid systems (combining passive and active anti-icing methods) with potential applications for UAVs operating in cold environments. The results showed that stand-alone thermal heating or anti-icing via super-/hydrophobic coatings are not sufficient for these applications. However, when synergized, they effectively prevent ice formation on airfoil surfaces, enhance icing mitigation, and reduce power requirements. This can lead to lower operational costs, extended maintenance periods, and improved safety in regions prone to icing conditions. Future work should focus on the coating's performance in de-icing tests and under rime-ice conditions (V_∞ = 20 m/s, T = -15°C and LWC = 0.5 g/m^3). Surface wettability measurements were then used to determine the overall durability of the coating, together with ice adhesion and surface roughness measurements. The coating exhibited degradation in terms of the contact angle and surface roughness and an increase in ice adhesion after 60 minutes of accelerated testing at V = 80 m/s and LWC = 16.0 g/m^3. However, the coating still remained hydrophobic and did not degrade all the way to the underlying enamel surface, showing that the WX-2100 coating is sufficiently durable.

Acknowledgments

The research work is partially supported by the Army Research Office (ARO) under the contract number of W911NF2410251 and National Science Foundation (NSF) under the award numbers of CBET-1935363 and CBET-2313310.

References

[1] Miziński, B., & Niedzielski, T. (2017). Fully-automated estimation of snow depth in near real time with the use of unmanned aerial vehicles without utilizing ground control points. Cold Regions Science and Technology, 138, 63-72.

[2] Siquig, R. A. "Impact of icing on unmanned aerial vehicle (UAV) operations." Naval environmental prediction research facility report (1990).

[3] Hann, R., & Johansen, T. A. (2020). Unsettled topics in unmanned aerial vehicle icing.

[4] Zhang, Z., Ma, L., Liu, Y., Ren, J., & Hu, H. (2021). An experimental study of rain erosion effects on a hydro-/ice-phobic coating pertinent to Unmanned-Arial-System (UAS) inflight icing mitigation. Cold Regions Science and Technology, 181, 103196.

[5] Asmatulu, R., Khan, W. S., Reddy, R. J., & Ceylan, M. (2015). Synthesis and analysis of injection-molded nanocomposites of recycled high-density polyethylene incorporated with graphene nanoflakes. Polymer Composites, 36(9), 1565-1573.

[6] He, Z., Xie, H., Jamil, M. I., Li, T., & Zhang, Q. (2022). Electro-/Photo-Thermal Promoted Anti-Icing Materials: A New Strategy Combined with Passive Anti-Icing and Active De-Icing. Advanced Materials Interfaces, 9(16), 2200275.

[7] Gao, Linyue, et al. "A hybrid strategy combining minimized leading-edge electric-heating and superhydro-/ice-phobic surface coating for wind turbine icing mitigation." Renewable energy 140 (2019): 943-956.

[8] Huang, Wuji, et al. "Superhydrophobic surface processing for metal 3D printed parts." Applied materials today 29 (2022): 101630.

[9] Farzam, Melika, et al. "Advances in the fabrication and characterization of superhydrophobic surfaces inspired by the Lotus leaf." Biomimetics 7.4 (2022): 196.

[10] Ma, Liqun, et al. "Bio-inspired icephobic coatings for aircraft icing mitigation: A critical review." Progress in Adhesion and Adhesives 6 (2021): 171-201.

[11] Ma, Liqun, et al. "An exploratory study on using Slippery-Liquid-Infused-Porous-Surface (SLIPS) for wind turbine icing mitigation." Renewable Energy 162 (2020): 2344-2360.

[12] Jackson, M.J., Field, J.E., (2000). Modelling liquid impact fracture thresholds in brittle materials. Br. Ceram. Trans. 99, 1–13. https://doi.org/10.1179/bct.2000.99.1.1.

[13] Slot, H.M., Gelinck, E.R.M., Rentrop, C., Van der Heide, E., (2015). Leading edge erosion of coated wind turbine blades: Review of coating life models. Renew. Energy 80, 837–848. https://doi.org/10.1016/j.renene.2015.02.036.

[14] Fujisawa, N., Takano, S., Fujisawa, K., Yamagata, T., (2018). Experiments on liquid droplet impingement erosion on a rough surface. Wear 398–399, 158–164. https://doi.org/10.1016/j.wear.2017.12.003.

[15] Ghidaoui, M.S., Zhao, M., McInnis, D.A., Axworthy, D.H., (2005). A review of water hammer theory and practice. Appl. Mech. Rev. 58, 49. https://doi.org/10.1115/1.1828050.

[16] Li, Linkai, et al. "Effects of thermal conductivity of airframe substrate on the dynamic ice accretion process pertinent to UAS inflight icing phenomena." International Journal of Heat and Mass Transfer 131 (2019): 1184-1195.

[17] Waldman, Rye M., and Hui Hu. "High-speed imaging to quantify transient ice accretion process over an airfoil." Journal of Aircraft 53.2 (2016): 369-377.

[18] Liu, Yang, and Hui Hu. "An experimental investigation on the unsteady heat transfer process over an ice accreting airfoil surface." International Journal of Heat and Mass Transfer 122 (2018): 707-718.

[19] Sista, Harsha et al. “Qualification of Ice Accretion Characteristics on a Wind Turbine Blade Model at High Liquid Water Content Levels Pertinent to Offshore Wind Turbine Icing Phenomena”, AIAA AVIATION FORUM 2022. 2022.

[20] Digavalli, Kiran, et al. "Unsteady Heat Transfer Characteristics of Aircraft Anti-/De-Icing with Continuous and Pulsed Surface Heating." AIAA AVIATION FORUM AND ASCEND 2024. 2024.

[21] Superhydrophobic coatings. CYTONIX. (2024). https://cytonix.com/pages/cytothane-superhydrophobic-coatings

[22] Korhonen, J. T., Huhtamäki, T., Ikkala, O., & Ras, R. H. (2013). Reliable measurement of the receding contact angle. Langmuir, 29(12), 3858-3863.

[23] Beemer, D.L., Wang, W., Kota, A.K., (2016). Durable gels with ultra-low adhesion to ice. J. Mater. Chem. A 4, 18253–18258. https://doi.org/10.1039/c6ta07262c.

[24] Meuler, A.J., Smith, J.D., Varanasi, K.K., Mabry, J.M., McKinley, G.H., Cohen, R.E., (2010). Relationships between Water Wettability and Ice Adhesion. ACS Appl. Mater. Interfaces 2, 3100–3110. https://doi.org/10.1021/am1006035.

[25] Tourkine, Piotr, Marie Le Merrer, and David Quéré. "Delayed freezing on water repellent materials." Langmuir 25.13 (2009): 7214-7216.

[26] Hu, Haiyang, et al. "Comparative Study of Using Superhydrophobic and Icephobic Surface Coatings for Aircraft Icing Mitigation." AIAA Journal 62.4 (2024): 1588-1600.